HHS Public Access

Author manuscript

Nat Med. Author manuscript; available in PMC 2014 February 01.

Published in final edited form as:

Nat Med. 2013 August ; 19(8): 1023–1029. doi:10.1038/nm.3216.

ETS factors reprogram the androgen receptor cistrome and prime prostate tumorigenesis in response to PTEN loss

Yu Chen[1,2,6], **Ping Chi**[1,2,6], **Shira Rockowitz**[3], **Phillip J. Iaquinta**[2], **Tambudzai Shamu**[2], **Shipra Shukla**[2], **Dong Gao**[2], **Inna Sirota**[2], **Brett S. Carver**[2], **John Wongvipat**[2], **Howard I. Scher**[1], **Deyou Zheng**[3,4], and **Charles L. Sawyers**[2,5]

[1]Department of Medicine, Memorial Sloan-Kettering Cancer Center, New York, New York, USA

[2]Human Oncology and Pathogenesis Program, Memorial Sloan-Kettering Cancer Center, New York, New York, USA

[3]Department of Genetics, Albert Einstein College of Medicine, Bronx, New York, USA

[4]Departments of Neurology and Neuroscience, Albert Einstein College of Medicine, Bronx, New York, USA

[5]Howard Hughes Medical Institute, Memorial Sloan-Kettering Cancer Center, New York, New York, USA

Abstract

Studies of ETS-mediated prostate oncogenesis have been hampered by the lack of suitable experimental systems. Here we describe a new conditional mouse model which gives robust, homogenous ERG expression throughout the prostate. When combined with homozygous *Pten* loss, mice developed accelerated, highly penetrant invasive prostate cancer. In mouse prostate tissue, ERG significantly increased androgen receptor (AR) binding. Robust ERG-mediated transcriptional changes, observed only in the setting of *Pten* loss, included restoration of AR transcriptional outut and genes involved in cell death, migration, inflammation and angiogenesis. Similarly, ETV1 positively regulated AR cistrome and transcriptional output in *ETV1*-translocated, *PTEN*-deficient human prostate cancer cells. In two large clinical cohorts, *ERG* and *ETV1* expression correlated with higher AR transcriptional output in *PTEN*-negative prostate cancer specimens. We propose that *ETS* factors cause prostate-specific transformation by altering the AR cistrome, priming the prostate epithelium to respond to aberrant upstream signals such as *PTEN* loss.

[6]These authors contributed equally

Author contributions: Y.C. and C.L.S. conceived of the project. Y.C. performed the mouse experiments with technical support from J.W., T.S. and D.G. P.C. performed expression profiling and ChIP-seq with technical support from S.S. and I.S. S.R. and D.Z. performed bioinformatic analysis. P.J.I. performed the LNCaP ETV1 knockdown experiments. B.S.C and H.I.S. provided major intellectual input for initial project design and further troubleshooting. Y.C., P.C. and C.L.S. wrote the manuscript.

Introduction

Translocations of ETS transcription factors *ERG*, *ETV1*, *ETV4*, *ETV5* and *FLI1* occur in half of all prostate cancer and the *TMPRSS2-ERG* translocation is the most common molecular alteration[1-4]. Evidence from human tumor analysis strongly implicates aberrant *ETS* expression as an early if not initiating event[5-7].

Transgenic mouse models have shown that neither *ERG* nor *ETV1* is sufficient to initiate prostate cancer[8-12]. Unfortunately, the existing probasin based transgenic *ETS* models are poorly suited for further mechanistic exploration, especially when combined with other genetic events that turn off probasin expression[9,13]. To overcome these shortcomings, we constructed a knock-in model of prostate-specific *ERG* expression that gives robust, uniform *ERG* expression throughout the mouse prostate. This model led us to the discovery that *ERG* reprograms the AR cistrome. These effects, in the context of *Pten* loss which suppresses AR, restore AR transcriptional activity and activate transcriptional targets involved in cell death, inflammation, migration and angiogenesis that result in rapid onset, widely invasive prostate cancer. Similarly, *ETV1* also alters the AR-cistrome and AR-transcriptional activity in *ETV1*-translocated, *PTEN*-negative prostate cancer cells. The findings reveal a previously unappreciated role for chromatin context in *ETS*-mediated transformation and offer a potential explanation for the tissue-restricted nature of *ETS* translocations.

Results

A robust mouse model of *ERG*-driven prostate cancer

We generated a conditional mouse of the *TMPRSS2-ERG* transgene knocked into the *Rosa26* locus ($R26^{ERG}$) (Supplementary Fig. 1). We crossed $R26^{ERG}$ with prostate specific *Pb-Cre4* mice to express *ERG* specifically in the prostate [14]. IHC against ERG or the IRES-linked EGFP showed that ERG was uniformly expressed in the ventral and dorsolateral lobes by 8 weeks and the anterior lobes by 3 months and that ERG did not affect AR expression (Fig. 1a, 2c, Supplementary Fig. 2). We did not appreciate any differences in prostate histology or cellular proliferation (Ki67 staining) in either heterozygous *Pb-Cre4;*$R26^{ERG/+}$ or homozygous *Pb-Cre4;*$R26^{ERG/ERG}$ mice up to 1 year of age. Approximately 50% of *ERG* mice older than 1 year exhibited focal ventral lobe hyperplasia (Fig. 1b, c). We conclude that ERG alone, even in the context of robust and high level protein expression is insufficient to cause prostate cancer[15-17].

Previously reported transgenic models of *ERG* expression in a *Pten* germline heterozygous background show prostatic intraepithelial neoplasia (PIN) that is patchy and variably penetrant[8,10,18]. We crossed $R26^{ERG}$ to $Pten^{flox}$ mice to generate double homozygous mice ($R26^{ERG}$;$Pten^{f/f}$). $Pten^{f/f}$ mice developed highly penetrant and homogenous PIN that does not progress to grossly invasive disease. In $Pten^{f/f}$;$R26^{ERG}$ mice, invasive adenocarcinoma characterized by small irregular glandular structures comprised of malignant cells with large, pleiomorphic nuclei and pale cytoplasm developed adjacent to PIN by 8 weeks (Supplementary Fig. 3).

By six months, approximately 80% of *Pten*$^{f/f}$;*R26*^{ERG} mice contained regions of adenocarcinoma with enlarged, hardened prostates (Fig. 2a, b). The tumor cells uniformly express nuclear ERG and AR, and display Akt activation (pAkt). While the invasive regions are highly proliferative, the proliferative index of PIN lesions in *Pten*$^{f/f}$;*R26*^{ERG} prostates is only slightly higher than those in *Pten*$^{f/f}$ prostates (Fig. 2c), suggesting that *ERG* expression within PIN does not significantly affect proliferation. Instead, *ERG* expression may facilitate invasion and progression, as suggested in earlier *in vitro* studies[16,18]. Human PIN retains a basal layer of p63 and cytokeratin 5 (CK5)-positive cells beneath a luminal layer of cytokeratin 8 (CK8)-positive cells whereas adenocarcinoma is characterized by irregular glandular structures that have lost the basal layer. In *Pten*$^{f/f}$ PIN, p63 and CK5 are maintained in the basal cells and CK5 is ectopically expressed in some luminal cells, consistent with prior reports (Supplementary Fig. 4)[19]. *Pten*$^{f/f}$;*R26*^{ERG} adenocarcinoma is invariably positive for CK8 and negative for p63 consistent with human adenocarcinoma. CK5 expression is variable and, when present, coincides with CK8 expression. CK5/8 double positive cells, coined as the “intermediate cells” are detectable in a subset of human prostate cancers[20].

By 12 months, some mice develop foci of poorly differentiated carcinoma that maintain expression of AR, ERG, and CK8 and display patchy neuroendocrine differentiation demonstrated by Nestin staining (Fig. 2d, Supplementary Fig. 5). These patterns are reminiscent of human Gleason 5 cancer with focal neuroendocrine differentiation, in contrast to “small cell” cancer characterized by loss of AR and uniform neuroendocrine staining. *Pten*$^{f/f}$;*R26*^{ERG} mice have shortened survival relative to *Pten*$^{f/f}$ mice (Fig. 2e), with early deaths due to increased abdominal girth and penile prolapse.

ERG reprograms the AR cistrome

The robust and uniform expression of ERG in *R26*^{ERG} and *Pten*$^{f/f}$;*R26*^{ERG} mice provides an ideal model to explore the ERG cistrome and transcriptome under controlled conditions. ChIP-seq analysis identified 24,665 ERG peaks in prostate tissue from *R26*^{ERG} mice (Supplementary Table 1). While most ERG peaks reside in the enhancer regions, they were enriched at promoters (30% versus 3% in genome-wide background, $p<2.2\times10^{-16}$) (Supplementary Fig. 6), consistent with prior ERG ChIP-seq[21,22]. ERG peaks were present in homologs of many well-characterized human ERG and ETV1 target genes such as *Dusp6*, *Tmprss2*, and *Fkbp5* that were defined in *ERG*-positive VCAP and *ETV1*-positive LNCaP cells (Fig. 3a, Supplementary Fig. 7, 8), giving us further confidence in the physiologic relevance of the mouse model. We observed similar distribution of ERG binding sites in the *Pten* loss background (Supplementary Fig. 9, 10).

We next examined the genome-wide localization of AR by ChIP-seq. Strikingly, there was a >4-fold increase in the number of AR peaks in *R26*^{ERG} (14,889) compared to *WT* prostates (3,476) (Fig. 3b, Supplementary Table 1). The number of AR peaks was also increased in *Pten*$^{f/f}$;*R26*^{ERG} prostates but to a lesser extent than in *Pten*^{wt} mice. We validated increased AR binding at several enhancers using ChIP-qPCR of independent samples (Supplementary Fig. 11). We confirmed that the change in the AR cistrome was not due to difference in AR protein or circulating testosterone (Fig. 1a, Supplementary Fig. 12, 13).

De novo MEME motif analysis[23] of ERG peaks identified the ETS core consensus GGAA motif with 5′-CC and 3′-GT bias identical to human prostate cancer cells. AR motif analysis showed that pre-existing sites in *WT* mice and new sites in *R26*^{ERG} mice contained the identical AR motif (Supplementary Fig. 14). To discover potential cooperating transcription factors for AR binding, we performed DREME analysis[24]. One distinguishing feature between conserved and new AR peaks was greater enrichment for GATA motifs in the new AR peaks and FOXA1 motifs in conserved AR peaks (Fig. 3c, Supplementary Table 2). This is of potential interest because GATA2 is essential for prostate development and cooperates with AR to modulate gene expression[25,26].

The percentage of AR and ERG peaks that physically co-localize in *R26*^{ERG} mouse prostates was ∼44% (Fig. 3d, left), which is highly significant and comparable to VCAP cells. Yet, new AR peaks have less overlap with ERG peaks than the conserved AR peaks (∼40% versus ∼60%, Fig. 3e, f), making it unlikely that ERG directly recruits AR to new sites. However, a large fraction of new AR sites (77%, $p < 1\times10^{-20}$) map to genes containing ERG sites, raising the possibility of an ERG-mediated field effect that promotes AR binding, perhaps by functioning as a pioneer factor.

Several classes of pioneer factors have been defined. One class, exemplified by the ETS factor PU.1, binds to closed chromatin regions and generates *de novo* enhancers, characterized by H3K4me1, which in turn guide recruitment of other transcription factors[27,28]. Another class, exemplified by FOXA1, binds to pre-established H3K4me1 enhancer regions and instructs binding of additional transcriptional factors (e.g. AR) to both adjacent and distant pre-existing enhancer regions[25,29,30]. To determine if ERG resembles one of these classes of pioneer factors, we examined the distribution of H3K4me1. The collective distribution of H3K4me1 around ERG binding sites was similar between wild-type and *R26*^{ERG} prostates, suggesting that ERG binds to pre-existing enhancers (Fig. 3g). Further, the collective distribution of H3K4me1 around both conserved and new AR peaks were also similar between wild-type and *R26*^{ERG} prostates, suggesting that ERG expression helps guide AR to pre-existing enhancers (Fig. 3h). Interestingly, the normalized H3K4me1 ChIP-signal was consistently slightly higher in *R26*^{ERG} mice for all three types of peaks (ERG, new AR and conserved AR), raising the possibility that ERG may strengthen pre-existing enhancers. Collectively, these data support a model whereby ERG reprograms the AR cistrome without significant changes in the K3K4me1 landscape.

ERG expression induces robust transcriptome changes in Pten loss background

We examined ERG-induced transcriptome changes in prostates from 4-month old *R26*^{ERG} mice and littermate controls and found only 20 genes changed by 1.5-fold with a FDR<0.3 cutoff, as appreciated by a volcano plot (including a 16-fold increase in ERG transgene linked EGFP) (Supplementary Fig. 15a, Supplementary Table 3).

However, in the *Pten*$^{f/f}$ background, *ERG* expression induced robust transcriptome changes, with greater than 800 genes significantly changed using the same criteria (Supplementary Fig. 15b, Supplementary Table 4). Principle component analysis of the 4 groups of mice showed that the first component is determined by *Pten* status and the second component is determined by *ERG* status (Fig. 4a). Unsupervised hierarchical clustering showed that *Pten*$^{f/f}$

prostates are clearly distinguished by *ERG* status. *Pten* intact prostates also clustered by *ERG* status though less robustly, consistent with the subtle transcriptome alterations (Fig. 4b). Closer examination of *ERG*-induced gene expression changes (ERG Δ) in the $Pten^{WT}$ versus the $Pten^{f/f}$ background revealed that *ERG* generally induced the same directional transcriptome changes that are greatly amplified in magnitude by *Pten* loss (Fig. 4a, b).

In $Pten^{f/f}$ prostates, both ERG up-regulated and ERG down-regulated genes were enriched with ERG and AR peaks (Supplementary Fig 16a, b). When we divided genes into those with only AR peaks, only ERG peaks, or both, only those with both were significantly enriched for regulation by ERG (Supplementary Fig. 16c–e). Among genes with AR peaks, those with "old" pre-existing AR peaks and those with "new" peaks found only in the setting of ERG expression are both enriched (Supplementary Fig. 16f, g). This data suggests that AR binding facilitates ERG-mediated transcriptional regulation. ERG-mediated upregulation of gene expression was also associated with increasing and widening of the H3K4me3 profile toward the gene body, a chromatin mark associated with active transcription[31], whereas ERG-mediated downregulation was associated narrowing and decreasing of the H3K4me3 peak (Supplementary Fig. 17a).

To determine whether ERG-induced transcriptome changes in the context of *Pten* loss resemble those observed in *ERG*-positive human prostate cancer, we used gene-set enrichment analysis (GSEA)[32] (Supplementary Table 5). Two ERG related human gene sets, one defined by genes upregulated in *ERG*-positive compared to *ERG*-negative human prostate cancer samples[33] and a second defined by genes down-regulated after *ERG* knockdown in VCAP cells[16], were highly enriched (Fig. 4c). Further evidence in support of the human relevance of the model comes from examination of specific genes such as adenosine monophosphate deaminase 3 (*AMPD3*), which is upregulated in both human and mouse *ERG*-positive prostate cancers. Conversely, trefoil factor 3 (*TFF3*)[34] is highly expressed in *ERG*-negative human prostate cancer and $Pten^{f/f}$ mouse prostate and down-regulated in *ERG*-positive human and $Pten^{f/f};R26^{/ERG}$ mouse prostate tumors (Fig. 4d, Supplementary Fig 17b).

The transcriptome heatmap reveals six distinct blocks of genes whose expression patterns vary as a group across genotypes. 2 groups can be primarily defined by genes upregulated by *Pten* loss (P^{up}), one of which is downregulated by ERG (P^{up}/E^{down}) and the other further upregulated by ERG (P^{up}/E^{up}). Similarly, there are 2 groups primarily defined by genes downregulated by *Pten* loss (P^{down}), one of which is further downregulated by ERG (P^{down}/E^{down}) and the other upregulated by ERG (P^{down}/E^{up}). Lastly, two additional groups of genes unchanged by *Pten* loss are primarily defined by up or downregulation by ERG (E^{up} or E^{down}). To understand the functional consequences of ERG expression, we performed pathway analysis of these distinct groups of genes using IPA and DAVID GO[35] (Supplementary Tables 6, 7). Among the most enriched processes in these groups are cell death (P^{up}/E^{down}), inflammation and migration (P^{up}/E^{up} group) and angiogenesis (E^{up}) (Fig. 4e). Identification of migration but not proliferation pathways is consistent with our histological evidence that ERG induces invasion without a change in Ki67 staining. The cell death finding agrees with prior work suggesting that *Pten* loss induces oncogenic stress[36], which may be alleviated by ERG expression.

ERG restores the AR transcriptome in mouse and human prostate cancers with *PTEN* loss

Having demonstrated that ERG induces dramatic changes in the AR cistrome, we asked if this resulted in changes in the AR transcriptome. GSEA revealed that two gene sets, one defined by genes down-regulated in mouse prostate with castration and another by genes induced by androgen in *ERG*-positive VCAP cells, were highly enriched by ERG expression in the $Pten^{f/f}$ background (Fig. 5a). As expected from prior work, *Pten* loss resulted in decreased expression of AR-regulated genes, as defined by castration experiments[9,37]. ERG expression had no significant effect on AR target genes in *Pten* intact mice but significantly restored AR transcriptional output in the setting of *Pten* loss (Fig. 5b, c). Since AR may regulate a distinct transcriptome in the setting of *Pten* loss, we performed a castration experiment of $Pten^{f/f}$ and $Pten^{f/f};R26^{ERG}$ mice (Supplementary Fig. 18). Expression profiling of the four groups of prostates show that genes downregulated by castration in the setting of *Pten* loss are upregulated by ERG expression, including established AR target genes such as probasin (*Pbsn*), *Nkx3-1*, and β-microseminoprotein (*Msmb*), all of which also correlate with the H3K4me3 profile that marks active transcription (Supplementary Fig. 19).

To determine the interaction of *Pten* loss and ETS expression in human prostate cancers, we turned to two large scale human prostate cancer gene expression data sets, one from the University of Michigan rapid autopsy series and one from the MSKCC prostatectomy series[7,33]. In both datasets, tumors with *PTEN* loss had a significantly decreased AR signature, consistent with prior reports. Further, in the setting of *PTEN* loss, *ETS*-positive tumors showed partial restoration of the AR signature (Fig. 5d). Thus, these analyses corroborate with experimental data that *ETS* overexpression positively regulates the *AR*-transcriptome in *PTEN* loss prostate cancer.

ETV1 modifies the AR cistrome and AR transcriptional activity

We next asked if the effects of ERG on AR DNA binding and transcriptional output described here are observed with other ETS family proteins targeted by prostate cancer translocations. The LNCaP prostate cancer cell line harbors an *ETV1* translocation and *PTEN*loss[11]. We performed ETV1 ChIP-seq in LNCaP cells and compared the binding sites with published ERG ChIP-seq data in VCAP cells[21]. ETV1 and ERG binding sites were highly similar, as 91% of ETV1 sites in LNCaP were bound by ERG in VCAP (Fig. 6a, see examples on **3a,** Supplementary Fig. 7, 8). Next, we examined the role of ETV1 in AR binding by performing AR ChIP-seq in LNCaP cells expressing an *ETV1*-specific shRNA (*ETV1sh2*) or a scrambled control[38]. *ETV1* knockdown resulted in a striking ∼90% decrease in the number of AR binding peaks (Fig. 6b, c, Supplementary Fig. 20). We validated this result by independent ChIP-qPCR experiments of the *PSA* and *TMPRSS2* enhancers with two different *ETV1* shRNAs and in the presence or absence of R1881 treatment (Supplementary Fig. 21). We next performed transcriptional profiling of *ETV1* knockdown using two shRNAs. *ETV1* knockdown reduced AR transcriptional activity measured both by AR output score and by GSEA which showed that the AR signature is the most enriched gene set (Fig. 6d, e, Supplementary Fig. 22, Supplementary Table 8). Thus, both ETV1 and ERG positively regulate AR binding and AR transcription in the context of *PTEN* loss.

Discussion

Previous transgenic models, while critical in establishing *ERG*'s oncogenic potential, are limited by the subtle phenotype and variable penetrance. Here we report a novel *ERG* knock-in model with uniform transgene expression in all prostate epithelial cells that gives highly predictable, early onset invasive prostate cancer when combined with *Pten* deficiency. These characteristics make this a broadly useful new model for the prostate cancer research community for mechanistic and therapeutic studies of *ERG*-driven prostate cancer.

An unanticipated finding is that ERG appears to function as a pioneer factor, causing dramatic changes in the AR cistrome. This property is not unique to ERG because knockdown of *ETV1* results in a similarly dramatic loss in AR binding sites. The large increase in AR binding sites seen in *ERG*-expressing mice cannot be explained solely by co-recruitment of AR by ERG to adjacent binding sites. However, the fact that ∼80% of the new AR sites map to genes that also contain ERG sites support a pioneer model whereby ERG causes local chromatin changes that facilitate AR binding to nearby but not adjacent sites. ChIP-seq studies of the H3K4me1 enhancer mark in prostate tissue from wild type mice establish that ERG primarily binds to pre-defined enhancers, presumably established during development of the genitourinary tract.

At the transcriptional level, the primary consequence of the *ERG*-driven changes in the AR cistrome is an increase in AR output, which is particularly evident in *Pten* deficient mice and in *PTEN*-negative human tumors. This requirement for additional signaling input to enhance the transcriptional effects of ERG is reminiscent of earlier work on the related ETS family protein ETV1 showing that KIT kinase activity amplifies *ETV1* transcriptional output in gastrointestinal stromal tumors[38].

Our conclusion that ERG enhances AR function contrasts with previous work showing that ERG suppresses AR function[21,22]. Potential explanations for these apparently contradictory findings include the fact that the earlier studies were conducted in VCAP cells, which are *PTEN*-intact and therefore may be less “sensitized” to the *ERG*-effect on *AR* transcriptome. Even in VCAP cells, there is evidence that ERG serves as a pioneer factor at a number of sites for AR binding including at the *SOX9* gene[39]. Further, *ERG* expression may impair differentiation, which can manifest as reduced expression of classic AR target genes associated with terminal prostate differentiation. Further work that comprehensively assesses the AR transcriptome in various contexts should clarify this.

In summary, *ERG* and *ETV1* mediate context-dependent oncogenic transformation by influencing the prostate lineage-specific master regulator, AR, and priming the prostate epithelium to cooperate with aberrant upstream signaling in prostate oncogenesis. Based on the increasing number of mutant transcription factors and chromatin modifiers emerging from cancer genome sequencing efforts, we speculate that the mechanism of oncogenesis described here for prostate cancer may be generalizable to other cancer types.

Supplementary Methods

Gene Targeting and mouse breeding

All mouse studies are approved by MSKCC IACUC under protocol 06-07-012. *Pb-Cre4*[9], and *Pten*$^{f/f}$[9] mice were previously described and all in the C57B6 background. Rosa26 targeting is described in Srinivas et. al.[40] with modifications (Supplementary Fig. 1). We started with with pBigT-invloxP (kind gift from Juan Pedro Martinez-Barbera) where the loxP sites were inverted in orientation to remove two sense ATG's that may aberrantly initiate translation prior to the *ERG* gene[41], and subsequently cloned the *TMPRSS2-ERG* cDNA containing non-coding exon 1 of human TMPRSS2 with exon 4 of ERG[8] and an IRES-nlsEGFP (Addgene plasmid 15037)[42] into the polycloning site respectively. This vector, pBigT-invloxP-ERG-IRES-nlsEGFP was cloned into Rosa26-Pam1 (Addgene 15036)[42]. The vector was targeted into 129 ES cells and injected into C57B6 blastocysts. Genotyping was performed using the following primers: R26-TA-WT-3F (5′-TCCCGACAAAACCGAAAATC-3′), R26-WT-3R (5′-AAGCACGTTTCCGACTTGAG-3′), ERG Ex7F (5′-CAAAACTCTCCACGGTTAATGC-3′), ERG Ex10R (5′-GCACTGTGGAAGGAGATGGT-3′) with wild-type band of 468 bp and targeted band of 205 bp.

To initially characterize gene expression, *Pb-Cre4;R26*$^{ERG/+}$ and *Pb-Cre4;R26*$^{ERG/ERG}$ mice were generated through standard mouse breeding. To facilitate breeding, upon generation of *R26*$^{ERG/ERG}$ homozygous mice, subsequent crosses involved *Pb-Cre4;R26*$^{ERG/ERG}$ males with *R26*$^{ERG/ERG}$ females that generated a 1:1 ratio of *Cre*$^{+}$ and *Cre*$^{-}$ mice. ChIP-seq and gene expression analysis were carried out in *R26*^{ERG} homozygous mice. To cross into the *Pten* conditional background, we crossed *Pb-Cre4;R26*$^{ERG/ERG}$ with *Pten*$^{f/f}$ mice and after two generations, obtained *Pb-Cre4;Pten*$^{f/+}$, *Pten*$^{f/f}$, *and Pb-Cre4;Pten*$^{f/+}$*;R26*$^{ERG/ERG}$, *Pten*$^{f/f}$*;R26*$^{ERG/ERG}$ mice. From these mice, subsequent breeding between *Pb-Cre4;Pten*$^{f/+}$ males and *Pten*$^{f/f}$ females generated *Pb-Cre4;Pten*$^{f/f}$ males (abbreviated as *Pten*$^{f/f}$ in text and figures) and breeding between *Pb-Cre4;Pten*$^{f/+}$*;R26*$^{ERG/ERG}$ males and *Pten*$^{f/f}$*;R26*$^{ERG/ERG}$ females generated *Pb-Cre4;Pten*$^{f/f}$*;R26*$^{ERG/ERG}$ males (abbreviated as *Pten*$^{f/f}$*;R26*^{ERG} in text and figures).

Mouse procedures

To measure serum testosterone level, blood was obtained immediately after CO2 euthanasia via cardiac puncture and testosterone ELISA was performed using a KIT from ALPCO. Mouse prostate dissection was performed as described[13]. For isolation of chromatin and RNA for *Pten* wild-type mice, all prostate lobes were pooled. For *Pten*$^{f/f}$ prostates, the ventral, lateral, and dorsal lobes were pooled as the anterior lobe was more cystic and frequently highly fibrotic. Mouse castration was performed as described[9] and RNA isolation was carried out 48 hours after castration.

Chromatin immunoprecipitation and sequencing

To isolate chromatin from mouse prostate, prostates from 6-month old mice were minced using scissors, and crosslinked using 1% paraformaldehyde for 15 minutes. Sample was

washed in PBS, resuspended in lysis buffer, and dounced in a Tenbroeck style tissue grounder prior to sonication and IP as previously described[38]. Chromatin isolation from LNCaP cells growing in FBS was performed as previously described[38]. For ETV1 knockdown experiments, chromatin was isolated 72-hours after lentiviral infection.

ChIP-qPCR primers for human *KLK3*, *TMPRSS2* were described[43]. Mouse ChIP-qPCR primers pairs are: *Tmprss2* enhancer (5′-GAGGCACTTTTTGCCCAGTG-3′, 5′-CCAGGATGTGTCTGGGGAAC-3′), *Fkbp5* enhancer (5′-TGTGGCTGGCACATGAACTCGA-3′, 5′-GCTGTATGCTCCCCACCCCC-3′), and *Nkx3-1* enhancer (5′-TGTTGACATGGCTTCCTCGT-3′, 5′-TGGTTTATCGCCGTACCTTT-3′).

Next generation sequencing was performed either on an Illumina Genome Analyzer 2 or HiSeq2000 with 50 base-pair single reads. Reads were aligned to either the mouse genome (mm9) or the human genome (hg 18) using the ELAND alignment software within the Illumina Analysis Pipeline and duplicate read were eliminated for subsequent analysis. Peak calling was performed using MACS 1.4[44] comparing IP chromatin with input chromatin. Based on RefSeq gene annotation, the resultant peaks were separated into promoter peaks (located within ± 2 kb of a transcription start site (TSS)), promoter distal peaks (located from -50 kb of a transcription start to + 5kb of a transcription end), and otherwise intergenic peaks. Genes with one or more peaks in their promoter or promoter distal (also referred to as "enhancer") regions were considered as AR or ERG targets. The MEME software suite[23] and DREME[24] were applied for motif analysis using 300-bp sequences centered on either AR or ERG peaks. ChIP-seq profiles are presented using Integrated Genome Browser software of SGR format files. For overlapping analysis of AR, ERG, H3K4me3, and H3K4me1 peaks, we defined two peaks overlap if they shared at least one base pair across their full peak spans, as detected by MACS.

RNA analysis

To isolate RNA from mouse prostates, freshly dissected 3-month old prostate tissue was immediately placed into Trizol and homogenized using a FastPrep-24 instrument with Lysing Matrix A (MP Biomedicals). After phase separation, the RNA fraction was further purified using RNAEasy Mini kit.

Gene expression profiling was performed as described[38] using the Illumina MouseWG-6 v2.0 Expression BeadChip (4-month old *WT*, $R26^{ERG}$, $Pten^{f/f}$ and $Pten^{f/f};R26^{ERG}$) and Illumina MouseRef-8 v2.0 Expression BeadChip (6-month old intact and castrate $Pten^{f/f}$ and $Pten^{f/f};R26^{ERG}$). Expression analysis was performed using Partek Genomics Suite. Significantly changed probes induced by ERG expression were defined as genes with a >1.5-fold change and a Benjamini–Hochberg FDR < 0.3.

For gene expression profiling of LNCaP cells, cells were infected using a scrambled or two ETV1-specific shRNAs in the PKO.1 backbone[38] in triplicates. RNA was harvested 72-hours after infection and profiled using Illumina HT-12 microarray. To obtain the AR signature score, the normalized expression of a set of canonical AR-regulated genes was summed[9].

Gene ontology analysis of ERG-regulated gene sets were performed using DAVID[35] and Ingenuity IPA (http://www.ingenuity.com). Gene set enrichment analysis was performed using the JAVA program (http://www.broadinstitute.org/gsea) as described[38]. For ERG profile in *Pten* loss mouse prostate, genes were ranked from most upregulated to most downregulated in $Pten^{f/f};R26^{ERG/ERG}$ mice compared to $Pten^{f/f}$ mice. For ETV1 profile in LNCaP cells, genes were ranked by the mean changed by two shETV1 hairpins compared to scrambled hairpin. We used the gene sets in the Molecular Signatures Database (MSigDB) and added the following: CARVER_CASTRATION_UP and CARVER_CASTRATION_DN defined by genes upregulated and downregulated >1.5-fold in the mouse prostate (GSE24691), TAYLOR_PCA_ERG_UP defined by genes with greater than 1.5-fold higher expression in *ERG*-positive compared to ERG-negative tumors (GSE21034)[33], VCAP_siERG_DN defined by genes downregulated >2-fold by siRNA against ERG, VCAP_R1881_UP defined by genes upregulated >3-fold by R1881 treatment[16], and AR_SIG is a set of canonical AR upregulated genes[9].To integrate transcriptome with cistrome, we analyzed the gene that was both present in the Illumina MouseWG-6 v2.0 microarray and mouse RefSeq (19,260 genes) and compared the percent of all 19,260 of these genes with ERG and AR peaks with perturbed genes with ERG or AR peaks.

We analyzed two human prostate cancer datasets, a rapid autopsy series from University of Michigan (GSE35988) employing Agilent 44K microarray and MSKCC prostatectomy series employing Affymetrix Human Exon 1.0 ST Array (GSE21034). *PTEN* loss is defined, *ERG* and *ETV1* status are defined as shown (Supplementary Fig. 23). AR signature score of each sample is the sum of normalized expression of each gene in a canonical AR signature[9] with the exception of *TMRPSS2* because many *ETS*-positive tumors contain a genomic deletion of *TMPRSS2* due to genomic fusion with the ETS partner.

Protein Analysis

The following antibodies were used for IHC, WB, and ChIP: rabbit AR (Epitomics clone ER179(2)), rabbit ERG (Epitomics clone EPR3864), rabbit ETV1[38], rabbit histone H3K4me1 (Abcam ab8895), rabbit AKT (Cell Signaling #4691), rabbit phospho-AKT (Cell Signaling #4060), rabbit Ki67 (Vector Labs #VP-K451), rabbit mouse smooth muscle actin (Sigma A5228), chicken EGFP (Abcam ab13970), mouse β-Actin (clone AC-15, Sigma), mouse GAPDH (clone 1D4, Santa Cruz), rabbit p63 (Epitomics clone EPR5701), rabbit CK5 (Covance), rabbit CK8 (Covance), and rabbit nestin (Abcam).

Tissue paraffin embedding, sectioning, and H&E staining was performed by MSKCC core facility. Immunohistochemistry was performed by the MSKCC molecular cytology core using a Ventana Discovery XT.

To generate lysates for Western blotting, tissue was homologized in RIPA buffer using FastPrep-24 system with Lysing Matrix A (MP Biomedicals).

Statistics

All statistical comparisons between two groups were performed by Graphpad Prism software used two-tailed unpaired t-test. Kaplan Meier analysis was performed by Graphpad Prism using Log-rank Mantel-Cox test.

Accession Codes

Gene expression and ChIP-seq data can be found online at the Gene Expression Omnibus with the following accession numbers.

- Gene expression of LNCaP cells infected with scrambled and two different lentiviral shRNA against ETV1: GSEXXXX.
- Gene expression comparing four cohorts of mouse prostates (*WT*, *R26*^{ERG}, *Pten*$^{f/f}$, and *Pten*$^{f/f}$*;R26*^{ERG}): GSEXXXX.
- Gene expression comparing the effect of castration on *Pten*$^{f/f}$, and *Pten*$^{f/f}$*;R26*^{ERG} mouse prostates: GSEXXXX.
- ChIP-seq of mouse prostates of the 4 cohorts (*WT*, *R26*^{ERG}, *Pten*$^{f/f}$, *and Pten*$^{f/f}$*;R26*^{ERG}) using the following antibodies (AR, ERG, H3K4me1, H3K4me3): GSEXXXX.
- ChIP-seq of steady state LNCaP cells (ETV1 and H3K4me1) and LNCaP cells infected with scrambled and *ETV1sh2* (AR): GSEXXXX.

Supplementary Material

Refer to Web version on PubMed Central for supplementary material.

Acknowledgments

We thank the follow MSKCC core facilities: Gene Targeting (C. Yang), Mouse Genetics Core (W. Mark and P. Romanienko), Genomics Core Laboratory (A. Viale), Molecular Cytogenetics (M. Leversha), and Molecular Cytology (K. Manova) and the Rockefeller University Genomics Core (S. Dewell).

This work is supported in part by the Howard Hughes Medical Institute (CLS), NCI (K08CA140946, YC), (1K08CA151660-01A1, PC), (U01 CA141502, CLS), (P50CA092629, CLS, BC), US DOD (W81XWH-10-1-0197), Prostate Cancer Foundation (YC, BC), Starr Cancer Consortium (YC, PC, CLS, DZ), NIMH (R21MH099452, DZ).

We thank Dr. J. P. Martinez-Barbera for plasmids and Drs. C. D. Allis, F. Giancotti, and J. Otero for conceptual input, Dr. N. Schultz for bioinformatics assistance, and Drs. A. Gopalan.and S. Couto for pathology input.

References

1. Tomlins SA, et al. Recurrent fusion of TMPRSS2 and ETS transcription factor genes in prostate cancer. Science. 2005; 310:644–648. [PubMed: 16254181]
2. Tomlins SA, et al. TMPRSS2:ETV4 gene fusions define a third molecular subtype of prostate cancer. Cancer Res. 2006; 66:3396–3400. [PubMed: 16585160]
3. Helgeson BE, et al. Characterization of TMPRSS2:ETV5 and SLC45A3:ETV5 gene fusions in prostate cancer. Cancer Res. 2008; 68:73–80. [PubMed: 18172298]
4. Paulo P, et al. FLI1 is a novel ETS transcription factor involved in gene fusions in prostate cancer. Genes Chromosomes Cancer. 2012; 51:240–249. [PubMed: 22081504]

5. Mosquera JM, et al. Characterization of TMPRSS2-ERG fusion high-grade prostatic intraepithelial neoplasia and potential clinical implications. Clin Cancer Res. 2008; 14:3380–3385. [PubMed: 18519767]
6. Borno ST, et al. Genome-wide DNA methylation events in TMPRSS2-ERG fusion-negative prostate cancers implicate an EZH2-dependent mechanism with miR-26a hypermethylation. Cancer discovery. 2012; 2:1024–1035. [PubMed: 22930729]
7. Grasso CS, et al. The mutational landscape of lethal castration-resistant prostate cancer. Nature. 2012; 487:239–243. [PubMed: 22722839]
8. King JC, et al. Cooperativity of TMPRSS2-ERG with PI3-kinase pathway activation in prostate oncogenesis. Nat Genet. 2009; 41:524–526. [PubMed: 19396167]
9. Carver BS, et al. Reciprocal Feedback Regulation of PI3K and Androgen Receptor Signaling in PTEN-Deficient Prostate Cancer. Cancer cell. 2011; 19:575–586. [PubMed: 21575859]
10. Casey OM, et al. TMPRSS2- Driven ERG Expression In Vivo Increases Self-Renewal and Maintains Expression in a Castration Resistant Subpopulation. PLoS One. 2012; 7:e41668. [PubMed: 22860005]
11. Tomlins SA, et al. Distinct classes of chromosomal rearrangements create oncogenic ETS gene fusions in prostate cancer. Nature. 2007; 448:595–599. [PubMed: 17671502]
12. Shin S, et al. Induction of prostatic intraepithelial neoplasia and modulation of androgen receptor by ETS variant 1/ETS-related protein 81. Cancer Res. 2009; 69:8102–8110. [PubMed: 19789348]
13. Clegg NJ, et al. MYC cooperates with AKT in prostate tumorigenesis and alters sensitivity to mTOR inhibitors. PLoS One. 2011; 6:e17449. [PubMed: 21394210]
14. Wu X, et al. Generation of a prostate epithelial cell-specific Cre transgenic mouse model for tissue-specific gene ablation. Mech Dev. 2001; 101:61–69. [PubMed: 11231059]
15. Zong Y, et al. ETS family transcription factors collaborate with alternative signaling pathways to induce carcinoma from adult murine prostate cells. Proc Natl Acad Sci U S A. 2009; 106:12465–12470. [PubMed: 19592505]
16. Tomlins SA, et al. Role of the TMPRSS2-ERG gene fusion in prostate cancer. Neoplasia. 2008; 10:177–188. [PubMed: 18283340]
17. Klezovitch O, et al. A causal role for ERG in neoplastic transformation of prostate epithelium. Proc Natl Acad Sci U S A. 2008; 105:2105–2110. [PubMed: 18245377]
18. Carver BS, et al. Aberrant ERG expression cooperates with loss of PTEN to promote cancer progression in the prostate. Nat Genet. 2009; 41:619–624. [PubMed: 19396168]
19. Wang S, et al. Pten deletion leads to the expansion of a prostatic stem/progenitor cell subpopulation and tumor initiation. Proc Natl Acad Sci U S A. 2006; 103:1480–1485. [PubMed: 16432235]
20. Verhagen AP, et al. Colocalization of basal and luminal cell-type cytokeratins in human prostate cancer. Cancer Res. 1992; 52:6182–6187. [PubMed: 1384957]
21. Yu J, et al. An Integrated Network of Androgen Receptor, Polycomb, and TMPRSS2-ERG Gene Fusions in Prostate Cancer Progression. Cancer Cell. 2010; 17:443–454. [PubMed: 20478527]
22. Chng KR, et al. A transcriptional repressor co-regulatory network governing androgen response in prostate cancers. EMBO J. 2012; 31:2810–2823. [PubMed: 22531786]
23. Bailey TL, et al. MEME SUITE: tools for motif discovery and searching. Nucleic Acids Res. 2009; 37:W202–208. [PubMed: 19458158]
24. Bailey TL. DREME: motif discovery in transcription factor ChIP-seq data. Bioinformatics. 2011; 27:1653–1659. [PubMed: 21543442]
25. Lupien M, et al. FoxA1 translates epigenetic signatures into enhancer-driven lineage-specific transcription. Cell. 2008; 132:958–970. [PubMed: 18358809]
26. Andreu-Vieyra C, et al. Dynamic nucleosome-depleted regions at androgen receptor enhancers in the absence of ligand in prostate cancer cells. Mol Cell Biol. 2011; 31:4648–4662. [PubMed: 21969603]
27. Heintzman ND, et al. Histone modifications at human enhancers reflect global cell-type-specific gene expression. Nature. 2009; 459:108–112. [PubMed: 19295514]

28. Heinz S, et al. Simple combinations of lineage-determining transcription factors prime cis-regulatory elements required for macrophage and B cell identities. Molecular cell. 2010; 38:576–589. [PubMed: 20513432]
29. Sahu B, et al. Dual role of FoxA1 in androgen receptor binding to chromatin, androgen signalling and prostate cancer. EMBO J. 2011; 30:3962–3976. [PubMed: 21915096]
30. Wang D, et al. Reprogramming transcription by distinct classes of enhancers functionally defined by eRNA. Nature. 2011; 474:390–394. [PubMed: 21572438]
31. Lien WH, et al. Genome-wide maps of histone modifications unwind in vivo chromatin states of the hair follicle lineage. Cell stem cell. 2011; 9:219–232. [PubMed: 21885018]
32. Subramanian A, et al. Gene set enrichment analysis: a knowledge-based approach for interpreting genome-wide expression profiles. Proc Natl Acad Sci U S A. 2005; 102:15545–15550. [PubMed: 16199517]
33. Taylor BS, et al. Integrative genomic profiling of human prostate cancer. Cancer Cell. 2010; 18:11–22. [PubMed: 20579941]
34. Rickman DS, et al. ERG cooperates with androgen receptor in regulating trefoil factor 3 in prostate cancer disease progression. Neoplasia. 2010; 12:1031–1040. [PubMed: 21170267]
35. Huang da W, Sherman BT, Lempicki RA. Systematic and integrative analysis of large gene lists using DAVID bioinformatics resources. Nat Protoc. 2009; 4:44–57. [PubMed: 19131956]
36. Chen Z, et al. Crucial role of p53-dependent cellular senescence in suppression of Pten-deficient tumorigenesis. Nature. 2005; 436:725–730. [PubMed: 16079851]
37. Mulholland DJ, et al. Cell autonomous role of PTEN in regulating castration-resistant prostate cancer growth. Cancer cell. 2011; 19:792–804. [PubMed: 21620777]
38. Chi P, et al. ETV1 is a lineage survival factor that cooperates with KIT in gastrointestinal stromal tumours. Nature. 2010; 467:849–853. [PubMed: 20927104]
39. Cai C, et al. ERG induces androgen receptor-mediated regulation of SOX9 in prostate cancer. J Clin Invest. 2013; 123:1109–1122. [PubMed: 23426182]
40. Srinivas S, et al. Cre reporter strains produced by targeted insertion of EYFP and ECFP into the ROSA26 locus. BMC Dev Biol. 2001; 1:4. [PubMed: 11299042]
41. Ivanova A, et al. In vivo genetic ablation by Cre-mediated expression of diphtheria toxin fragment A. Genesis. 2005; 43:129–135. [PubMed: 16267821]
42. Murtaugh LC, Stanger BZ, Kwan KM, Melton DA. Notch signaling controls multiple steps of pancreatic differentiation. Proc Natl Acad Sci U S A. 2003; 100:14920–14925. [PubMed: 14657333]
43. Scher HI, et al. Antitumour activity of MDV3100 in castration-resistant prostate cancer: a phase 1-2 study. Lancet. 2010; 375:1437–1446. [PubMed: 20398925]
44. Zhang Y, et al. Model-based analysis of ChIP-Seq (MACS). Genome Biol. 2008; 9:R137. [PubMed: 18798982]

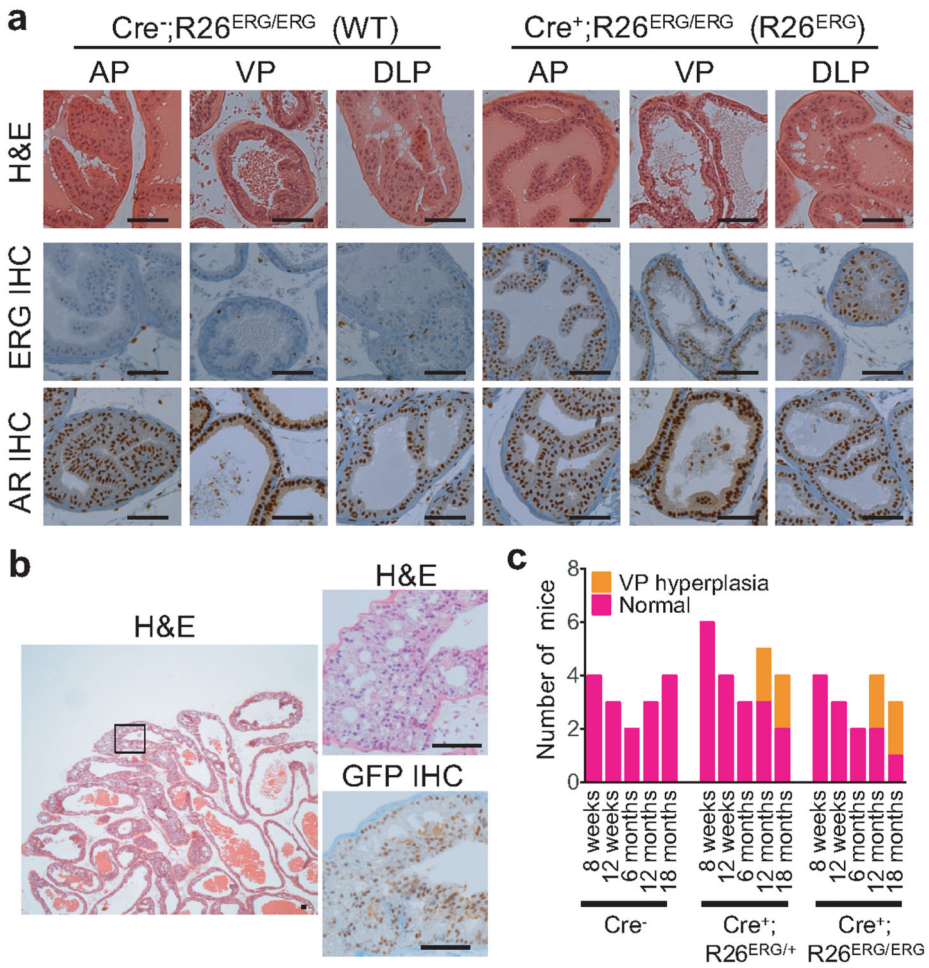

Figure 1. ERG expression induces minimal histological phenotype in mouse prostates

(a) Representative H&E histology, ERG IHC, and AR IHC of the anterior, ventral and dorsolateral (AP, VP and DLP) lobes in a 3-month old *Pb-Cre4;R26*$^{ERG/ERG}$(*R26*^{ERG}) and a littermate control *Cre*-negative (*WT*) mouse prostates. Scale bars: 50 μm. **(b)** A representative low-power H&E histology image of VP hyperplasia in the prostate of a 13-month old *R26*^{ERG} mouse is shown on the left. High power magnification of boxed region, including H&E and EGFP IHC, is shown on the right is shown on right. Scale bars: 50 μm. **(c)** Summary of histological findings of *WT* (*Cre*$^{+}$), *ERG* heterozygous (*Cre*$^{+}$*;R26*$^{ERG/+}$) and *ERG* homozygous (*Cre*$^{+}$; *R26*$^{ERG/ERG}$) mouse prostates examined at 8 and 12 weeks, 6, 12 and 18 months respectively.

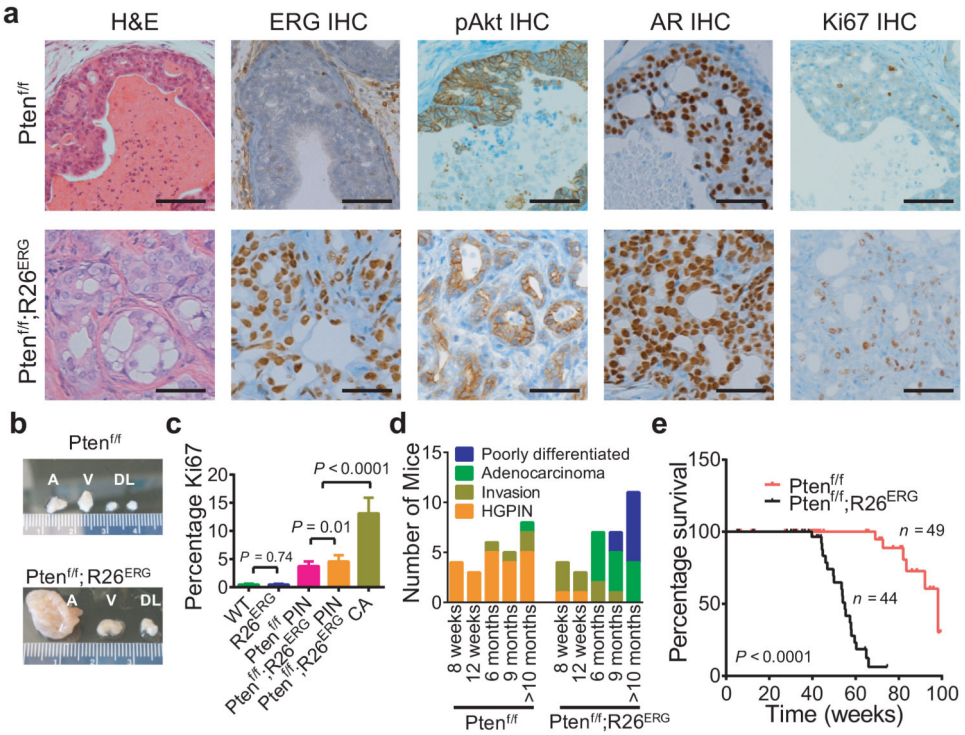

Figure 2. ERG robustly cooperates with Pten loss in prostate tumorigenesis

(a) Comparison of H&E prostate histology, ERG IHC, phosphorylated AKT (pAKT) IHC, AR IHC and Ki67 IHC of representative 6-month old *Cre*$^{+}$;*Pten*$^{f/f}$ (*Pten*$^{f/f}$) and *Cre*$^{+}$;*Pten*$^{f/f}$;*R26*$^{ERG/ERG}$ (*Pten*$^{f/f}$;*R26*^{ERG}) prostate. Scale bars: 50 μm. **(b)** A Representative example of gross appearance of anterior (A), ventral (V), dorsolateral (DL) lobes of *Pten*$^{f/f}$ and *Pten*$^{f/f}$;*R26*^{ERG} mice euthanized at 6 months. **(c)** Quantification of Ki67 (3 mice, 3 20× fields per mouse, mean ± SD) of 6-month old *WT*, *R26*^{ERG}, *Pten*$^{f/f}$ and *Pten*$^{f/f}$;*R26*^{ERG} mouse prostates. For *Pten*$^{f/f}$;*R26*^{ERG} mice, we separately quantified the PIN which is histologically similar to that of *Pten*$^{f/f}$ mice, and adenocarcinoma. **(d)** Summary of histological findings of *Pten*$^{f/f}$ and *Pten*$^{f/f}$;*R26*^{ERG} mouse prostates examined at 8 and 12 weeks, 6, 9 and >10 months respectively. Mice were characterized by the most advanced finding found on histology. **(e)** Kaplan-Meier survival analysis of *Pten*$^{f/f}$ and *Pten*$^{f/f}$;*R26*^{ERG} mice.

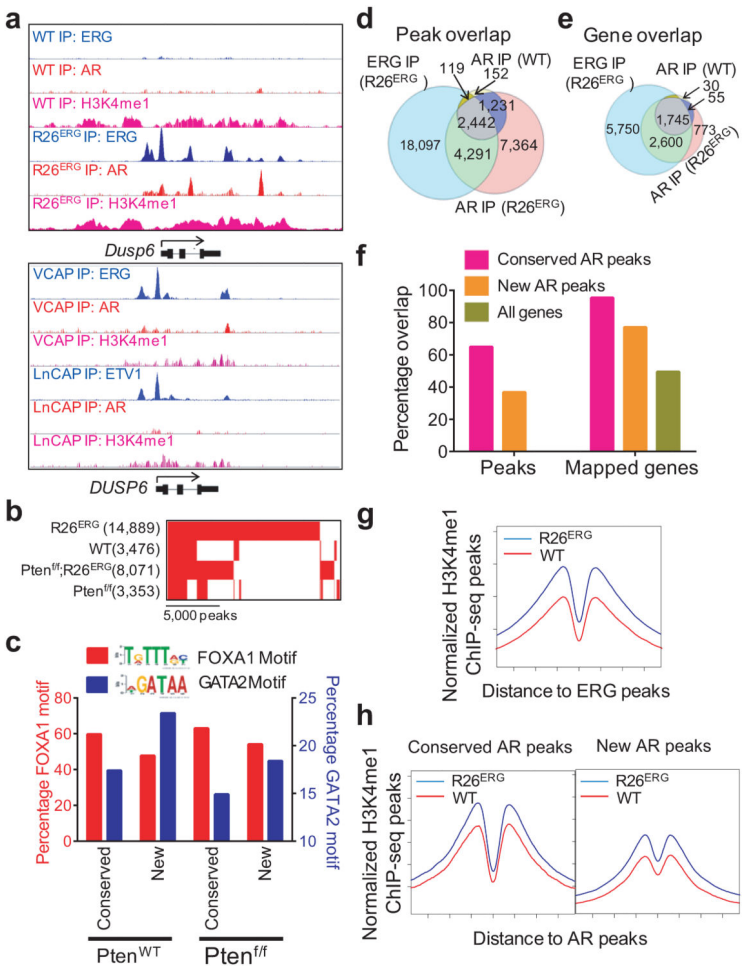

Figure 3. ERG localizes to pre-defined H3K4me1 marked regions and reprograms genome-wide localization of AR

(a) Representative ChIP-seq profiles of ERG, AR, and H3K4me1 at the *Dusp6* gene locus in *WT* and *R26*^{ERG} mouse prostates and at the human *DUSP6* gene locus in the *ERG*-positive VCAP and the *ETV1*-positive LNCaP human prostate cancer cell lines. **(b)** Overlap of AR peaks in *WT*, *R26*^{ERG}, *Pten*$^{f/f}$ and *Pten*$^{f/f}$*;R26*^{ERG} mouse prostates. Number of peaks is in parenthesis. **(c)** Bar graph of percentage of conserved AR peaks in ERG-negative mice and new AR peaks only in ERG-positive mice that have nearby FOXA1 (red, left y-axis) and GATA2 (blue, right y-axis) motifs in *Pten*^{WT} and *Pten*$^{f/f}$ prostates. **(d)** Venn diagram of ERG ChIP-seq peaks in *R26*^{ERG} mice, AR-ChIP-seq peaks in *WT* mice, and AR-ChIP-seq peaks in *R26*^{ERG} mice. Overlap of ERG and AR peaks in both *WT* and *R26*^{ERG} mice are significant ($P < 2.2\times10^{-16}$). **(e)** Overlap of mapped genes of ERG and AR peaks in *WT* and *R26*^{ERG} mouse prostates. **(f)** LEFT: Graph of the percent of conserved AR peaks in *WT* mice and new AR peaks in *R26*^{ERG} mice that overlap with ERG peaks in *R26*^{ERG} mice. RIGHT: Graph of percent of mapped genes of conserved AR peaks, of new AR peaks, and of all Refseq genes that overlap with mapped genes of ERG peaks. **(g)** Profiles of H3K4me1 ChIP-seq in *WT* and *R26*^{ERG} mouse around ERG binding sites of *R26*^{ERG} mice. **(h)** Profiles of H3K4me1 ChIP-seq associated with the conserved AR binding sites (left panel) and new

AR binding sites (right panel) induced by ERG expression in *R26*^{ERG} compared to *WT* mouse prostates.

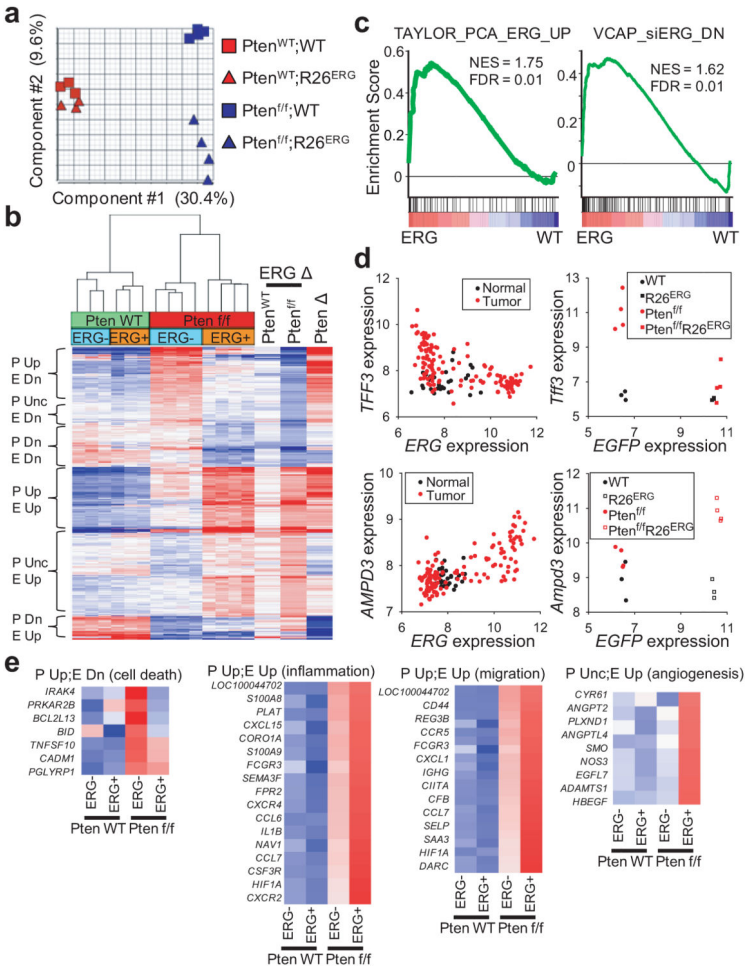

Figure 4. ERG expression primes prostate to respond to Pten loss

(a) Principle component analysis of expression profile of 4-month old *WT*, *R26*^{ERG}, *Pten*$^{f/f}$, and *Pten*$^{f/f}$*;R26*^{ERG} mouse prostates. Component 1 is determined by *Pten* status and component 2 by *ERG* status. **(b)** Hierarchical clustering of genes significantly changed either between *WT* and *R26*^{ERG} or between *Pten*$^{f/f}$ and *Pten*$^{f/f}$*;R26*^{ERG} mouse prostates (FDR<0.3, fold-change > 1.5). Clustering groups the genes by effect of Pten loss [Pten loss up (P Up), Pten loss unchanged (P Unc), Pten loss down (P Dn)] and ERG expression [ERG up (E Up), ERG down (E Dn)]. The three vertical heatmaps on the right show the fold-change of ERG expression in *WT* mice (between *WT* and *R26*^{ERG}) and in *Pten*$^{f/f}$ mice (between *Pten*$^{f/f}$ and *Pten*$^{f/f}$*;R26*^{ERG}) and effect of Pten loss in *ERG*-negative mice. **(c)** GSEA of the *ERG* expression profile in *Pten* loss mouse prostates (*Pten*$^{f/f}$*;R26*^{ERG} vs. *Pten*$^{f/f}$) showing that a gene set defined by *ERG*-positive vs. *ERG*-negative human prostate cancers[33] (Taylor_PCA_ERG_UP) and a gene set defined by genes down-regulated after *ERG* knockdown in VCAP cells[1616] (VCAP_siERG_DN) are positively enriched. **(d)** Scatter plot of *ERG* vs. *TFF3* and *ERG* vs *AMPD3* expression in human prostate cancer and normal prostate tissue (left) and scatter plot of *EGFP* (linked to ERG via IRES) vs *Tff3* and *EGFP* vs *Ampd3* expression in mouse prostate (right). **(e)** Normalized expression of genes

that belong to cell death, inflammation, migration, and angiogenesis functional groups that are regulated by ERG and Pten loss.

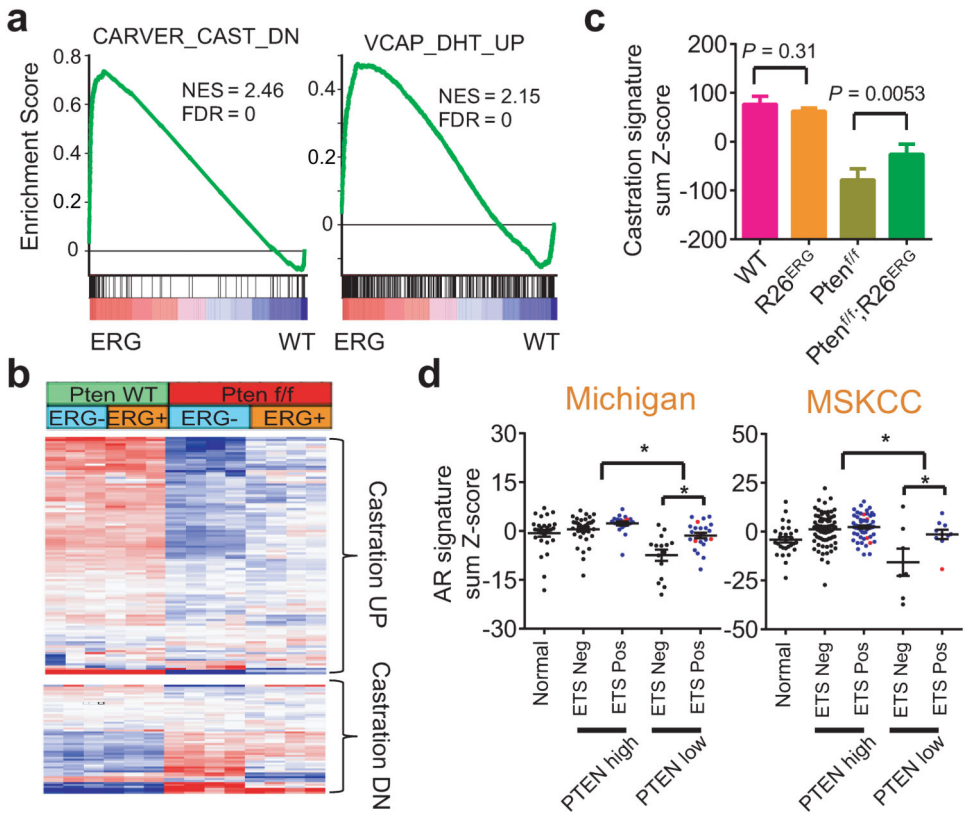

Figure 5. ERG increases androgen receptor signaling in Pten loss prostate cancer

(a) GSEA of the *ERG* expression profile in *Pten* loss mouse prostates (*Pten*$^{f/f}$;*R26*^{ERG} vs. *Pten*$^{f/f}$) showing that the mouse prostate specific AR-dependent gene set (defined by changes from mouse castration) and human AR-dependent gene set (defined by genes upregulated by DHT in ERG-positive VCAP cells) are both significantly and positively enriched. **(b)** Hierarchical clustering of mouse androgen upregulated genes (Castration DN) and androgen downregulated genes (Castration UP) in mouse prostates. The data shows that many androgen upregulated genes are downregulated by Pten loss and restored by ERG expression and many androgen downregulated genes are upregulated by Pten loss and decreased by ERG expression. **(c)** The sum of the normalized expression of mouse androgen-regulated genes, defined as genes downregulated by castration, by genotype (mean ± SD). **(d)** Sum of normalized expression of human androgen-regulated genes from University of Michigan (UM) rapid autopsy series and MSKCC prostatectomy series. Black dots, blue dots, and red dots represent ETS-negative, *ERG*-positive, and *ETV1*-positive samples respectively (mean ± SEM). For UM series, significant comparisons are: *PTEN* high vs. *PTEN* low ($P < 0.0001$) and *PTEN* low;ETS neg vs *PTEN* low;ETS pos ($P = 0.001$). For MSKCC series, significant comparisons are: *PTEN* high vs. *PTEN* low ($P < 0.0001$) and *PTEN* low;ETS neg vs *PTEN* low;ETS pos ($P = 0.043$).

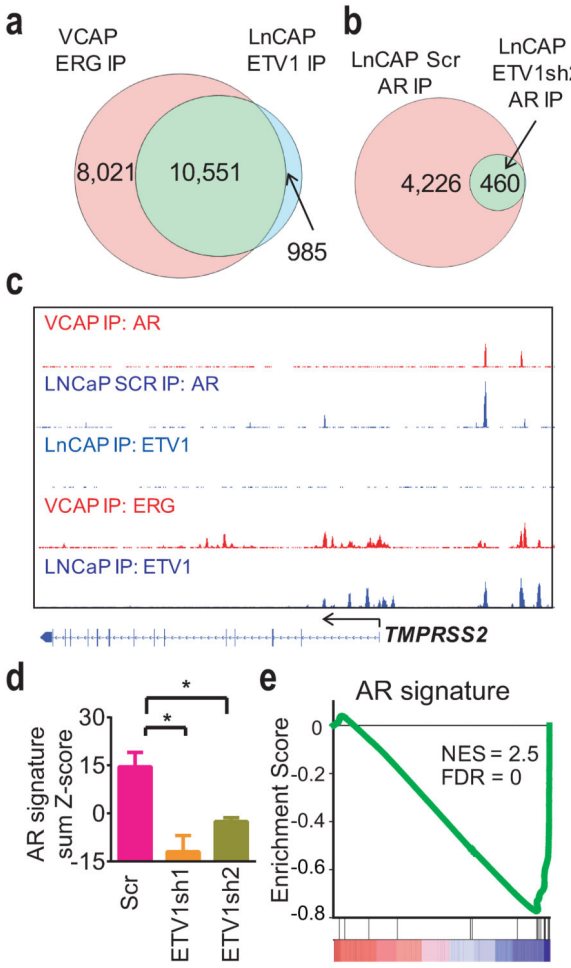

Figure 6. ETV1 alters the AR cistrome and the AR-dependent transcriptome LNCaP cells

(a) Overlap of ETV1 ChIP-seq peaks in LNCaP cells with published ERG ChIP-seq peaks in VCAP cells[21]. **(b)** Overlap of AR ChIP-seq peaks in LNCaP cells 72-hours after infection with scrambled shRNA and ETV1sh2 shRNA. **(c)** Representative ChIP-seq profile at the *TMPRSS2* locus showing ERG and AR profiles in VCAP cells and ETV1 baseline profile in LNCaP cells and AR profiles LNCaP cells infected with scrambled and ETV1sh2 shRNA. **(d)** The sum of normalized expression of genes in an AR signature from expression profiling in LNCaP cells 72-hours after infection with scrambled and two ETV1 shRNAs (n = 3, mean ± SD). Significant comparisons are Scr vs ETV1sh1 (P = 0.0026) and Scr vs ETV1sh2 (P = 0.0033). **(e)** GSEA profile showing that the AR signature gene set is highly enriched among genes downregulated by ETV1 knockdown.